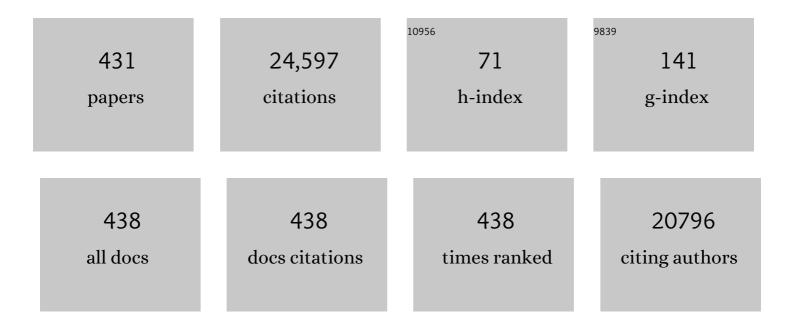
Simon Keith Warfield

List of Publications by Year in descending order

Source: https://exaly.com/author-pdf/6060992/publications.pdf Version: 2024-02-01



#	Article	IF	CITATIONS
1	Abnormal development of transient fetal zones in mild isolated fetal ventriculomegaly. Cerebral Cortex, 2023, 33, 1130-1139.	1.6	9
2	Reducing the Effects of Motion Artifacts in fMRI: A Structured Matrix Completion Approach. IEEE Transactions on Medical Imaging, 2022, 41, 172-185.	5.4	5
3	Superâ€resolution reconstruction of T2â€weighted thickâ€slice neonatal brain MRI scans. Journal of Neuroimaging, 2022, 32, 68-79.	1.0	8
4	Selfâ€supervised IVIM DWI parameter estimation with a physics based forward model. Magnetic Resonance in Medicine, 2022, 87, 904-914.	1.9	20
5	Scan-Specific Generative Neural Network for MRI Super-Resolution Reconstruction. IEEE Transactions on Medical Imaging, 2022, 41, 1383-1399.	5.4	15
6	Associations of body composition with regional brain volumes and white matter microstructure in very preterm infants. Archives of Disease in Childhood: Fetal and Neonatal Edition, 2022, 107, 533-538.	1.4	11
7	Fetal Brain Volume Predicts Neurodevelopment in Congenital Heart Disease. Circulation, 2022, 145, 1108-1119.	1.6	56
8	Normal Growth, Sexual Dimorphism, and Lateral Asymmetries at Fetal Brain MRI. Radiology, 2022, 303, 162-170.	3.6	24
9	Deep learning of birth-related infant clavicle fractures: a potential virtual consultant for fracture dating. Pediatric Radiology, 2022, 52, 2206-2214.	1.1	3
10	LGG-32. Integrated biologic, radiologic and clinical analysis of pediatric low-grade gliomas during and after targeted therapy treatment. Neuro-Oncology, 2022, 24, i95-i95.	0.6	0
11	Associations of Macronutrient Intake Determined by Point-of-Care Human Milk Analysis with Brain Development among very Preterm Infants. Children, 2022, 9, 969.	0.6	6
12	Diffusion-derived parameters in lesions, peri-lesion and normal-appearing white matter in multiple sclerosis using tensor, kurtosis and fixel-based analysis. Journal of Cerebral Blood Flow and Metabolism, 2022, 42, 2095-2106.	2.4	2
13	A structural brain network of genetic vulnerability to psychiatric illness. Molecular Psychiatry, 2021, 26, 2089-2100.	4.1	27
14	Regional Brain Growth Trajectories in Fetuses with Congenital Heart Disease. Annals of Neurology, 2021, 89, 143-157.	2.8	49
15	Dynamic distortion correction for functional MRI using FID navigators. Magnetic Resonance in Medicine, 2021, 85, 1294-1307.	1.9	16
16	Modeling dynamic radial contrast enhanced MRI with linear time invariant systems for motion correction in quantitative assessment of kidney function. Medical Image Analysis, 2021, 67, 101880.	7.0	7
17	Free induction decay navigator motion metrics for prediction of diagnostic image quality in pediatric MRI. Magnetic Resonance in Medicine, 2021, 85, 3169-3181.	1.9	2
18	Tractography of the Cerebellar Peduncles in Second- and Third-Trimester Fetuses. American Journal of Neuroradiology, 2021, 42, 194-200.	1.2	4

#	Article	IF	CITATIONS
19	Tuber Locations Associated with Infantile Spasms Map to a Common Brain Network. Annals of Neurology, 2021, 89, 726-739.	2.8	24
20	Magnetic Resonance Imaging (MRI) and Spectroscopy in Succinic Semialdehyde Dehydrogenase Deficiency. Journal of Child Neurology, 2021, 36, 1162-1168.	0.7	12
21	Free-breathing radial stack-of-stars three-dimensional Dixon gradient echo sequence in abdominal magnetic resonance imaging in sedated pediatric patients. Pediatric Radiology, 2021, 51, 1645-1653.	1.1	7
22	Association between Quantitative MR Markers of Cortical Evolving Organization and Gene Expression during Human Prenatal Brain Development. Cerebral Cortex, 2021, 31, 3610-3621.	1.6	11
23	Magic DIAMOND: Multi-fascicle diffusion compartment imaging with tensor distribution modeling and tensor-valued diffusion encoding. Medical Image Analysis, 2021, 70, 101988.	7.0	9
24	Physicsâ€based iterative reconstruction for dualâ€source and flying focal spot computed tomography. Medical Physics, 2021, 48, 3595-3613.	1.6	2
25	Fast and High-Resolution Neonatal Brain MRI Through Super-Resolution Reconstruction From Acquisitions With Variable Slice Selection Direction. Frontiers in Neuroscience, 2021, 15, 636268.	1.4	13
26	Transfer learning in medical image segmentation: New insights from analysis of the dynamics of model parameters and learned representations. Artificial Intelligence in Medicine, 2021, 116, 102078.	3.8	66
27	Matched neurofeedback during fMRI differentially activates rewardâ€related circuits in active and sham groups. Journal of Neuroimaging, 2021, 31, 947-955.	1.0	1
28	A machine learning-based method for estimating the number and orientations of major fascicles in diffusion-weighted magnetic resonance imaging. Medical Image Analysis, 2021, 72, 102129.	7.0	10
29	Spatiotemporal changes in diffusivity and anisotropy in fetal brain tractography. Human Brain Mapping, 2021, 42, 5771-5784.	1.9	14
30	Learning to estimate the fiber orientation distribution function from diffusion-weighted MRI. NeuroImage, 2021, 239, 118316.	2.1	17
31	Deep learning-based parameter estimation in fetal diffusion-weighted MRI. NeuroImage, 2021, 243, 118482.	2.1	22
32	MRI Super-Resolution Through Generative Degradation Learning. Lecture Notes in Computer Science, 2021, 12906, 430-440.	1.0	5
33	Retrospective Distortion and Motion Correction for Freeâ€Breathing DWâ€MRI of the Kidneys Using Dualâ€Echo EPI and Sliceâ€toâ€Volume Registration. Journal of Magnetic Resonance Imaging, 2021, 53, 1432-1443.	1.9	6
34	Parent-reported measure of repetitive behavior in Phelan-McDermid syndrome. Journal of Neurodevelopmental Disorders, 2021, 13, 53.	1.5	6
35	Gradient-Guided Isotropic MRI Reconstruction From Anisotropic Acquisitions. IEEE Transactions on Computational Imaging, 2021, 7, 1240-1253.	2.6	2
36	Quantitative In vivo MRI Assessment of Structural Asymmetries and Sexual Dimorphism of Transient Fetal Compartments in the Human Brain. Cerebral Cortex, 2020, 30, 1752-1767.	1.6	40

#	Article	IF	CITATIONS
37	Retrospective correction of head motion using measurements from an electromagnetic tracker. Magnetic Resonance in Medicine, 2020, 83, 427-437.	1.9	18
38	Rapid measurement and correction of spatiotemporal B ₀ field changes using FID navigators and a multiâ€channel reference image. Magnetic Resonance in Medicine, 2020, 83, 575-589.	1.9	23
39	Bulk motionâ€compensated DCEâ€MRI for functional imaging of kidneys in newborns. Journal of Magnetic Resonance Imaging, 2020, 52, 207-216.	1.9	11
40	Lesion-Constrained Electrical Source Imaging. Journal of Clinical Neurophysiology, 2020, 37, 79-86.	0.9	3
41	The Connectivity Fingerprint of the Fusiform Gyrus Captures the Risk of Developing Autism in Infants with Tuberous Sclerosis Complex. Cerebral Cortex, 2020, 30, 2199-2214.	1.6	11
42	Feed and wrap magnetic resonance urography provides anatomic and functional imaging in infants without anesthesia. Journal of Pediatric Urology, 2020, 16, 116-120.	0.6	14
43	Cross-scanner and cross-protocol multi-shell diffusion MRI data harmonization: Algorithms and results. NeuroImage, 2020, 221, 117128.	2.1	54
44	Association of Isolated Congenital Heart Disease with Fetal Brain Maturation. American Journal of Neuroradiology, 2020, 41, 1525-1531.	1.2	22
45	Dynamic Missing-Data Completion Reduces Leakage of Motion Artifact Caused by Temporal Filtering that Remains After Scrubbing. , 2020, , .		Ο
46	SLIMM: Slice localization integrated MRI monitoring. NeuroImage, 2020, 223, 117280.	2.1	6
47	In vivo characterization of emerging white matter microstructure in the fetal brain in the third trimester. Human Brain Mapping, 2020, 41, 3177-3185.	1.9	28
48	Simultaneous Motion and Distortion Correction Using Dualâ€Echo Diffusionâ€Weighted MRI. Journal of Neuroimaging, 2020, 30, 276-285.	1.0	9
49	Learning to Detect Brain Lesions from Noisy Annotations. , 2020, 2020, 1910-1914.		5
50	Pilot Study of Neurodevelopmental Impact of Early Epilepsy Surgery in Tuberous Sclerosis Complex. Pediatric Neurology, 2020, 109, 39-46.	1.0	23
51	Deep learning with noisy labels: Exploring techniques and remedies in medical image analysis. Medical Image Analysis, 2020, 65, 101759.	7.0	320
52	Spatiotemporal Differences in the Regional Cortical Plate and Subplate Volume Growth during Fetal Development. Cerebral Cortex, 2020, 30, 4438-4453.	1.6	22
53	Myofiber organization in the failing systemic right ventricle. Journal of Cardiovascular Magnetic Resonance, 2020, 22, 49.	1.6	3
54	Diffusion Tensor Imaging Abnormalities in the Uncinate Fasciculus and Inferior Longitudinal Fasciculus in Phelan-McDermid Syndrome. Pediatric Neurology, 2020, 106, 24-31.	1.0	9

#	Article	IF	CITATIONS
55	Prospective pediatric study comparing glomerular filtration rate estimates based on motion-robust dynamic contrast-enhanced magnetic resonance imaging and serum creatinine (eGFR) to 99mTc DTPA. Pediatric Radiology, 2020, 50, 698-705.	1.1	10
56	In vivo characterization of emerging white matter microstructure in the fetal brain in the third trimester. , 2020, 41, 3177.		4
57	Learning a Gradient Guidance for Spatially Isotropic MRI Super-Resolution Reconstruction. Lecture Notes in Computer Science, 2020, 12262, 136-146.	1.0	13
58	A Flux-Conservative Finite Difference Scheme for Anisotropic Bioelectric Problems. , 2020, , 135-146.		2
59	Head motion measurement and correction using <scp>FID</scp> navigators. Magnetic Resonance in Medicine, 2019, 81, 258-274.	1.9	40
60	Changes in neonatal regional brain volume associated with preterm birth and perinatal factors. NeuroImage, 2019, 185, 654-663.	2.1	45
61	Biomechanical modeling and computer simulation of the brain during neurosurgery. International Journal for Numerical Methods in Biomedical Engineering, 2019, 35, e3250.	1.0	20
62	Reproducibility of Structural and Diffusion Tensor Imaging in the TACERN Multi-Center Study. Frontiers in Integrative Neuroscience, 2019, 13, 24.	1.0	32
63	Increased electroencephalography connectivity precedes epileptic spasm onset in infants with tuberous sclerosis complex. Epilepsia, 2019, 60, 1721-1732.	2.6	37
64	Resting‣tate fMRI Networks in Children with Tuberous Sclerosis Complex. Journal of Neuroimaging, 2019, 29, 750-759.	1.0	6
65	White matter mean diffusivity correlates with myelination in tuberous sclerosis complex. Annals of Clinical and Translational Neurology, 2019, 6, 1178-1190.	1.7	24
66	Motion-corrected foetal cardiac MRI. Nature Biomedical Engineering, 2019, 3, 852-854.	11.6	1
67	Extra-axonal restricted diffusion as an in-vivo marker of reactive microglia. Scientific Reports, 2019, 9, 13874.	1.6	10
68	Suite of meshless algorithms for accurate computation of soft tissue deformation for surgical simulation. Medical Image Analysis, 2019, 56, 152-171.	7.0	52
69	Muti-shell Diffusion MRI Harmonisation and Enhancement Challenge (MUSHAC): Progress and Results. Mathematics and Visualization, 2019, , 217-224.	0.4	12
70	Perioperatively Inhaled Hydrogen Gas Diminishes Neurologic Injury Following Experimental Circulatory Arrest in Swine. JACC Basic To Translational Science, 2019, 4, 176-187.	1.9	15
71	Multi-Resolution Graph Based Volumetric Cortical Basis Functions From Local Anatomic Features. IEEE Transactions on Biomedical Engineering, 2019, 66, 3381-3392.	2.5	3
72	Tuberous Sclerosis Complex Genotypes and Developmental Phenotype. Pediatric Neurology, 2019, 96, 58-63.	1.0	21

#	Article	IF	CITATIONS
73	Intelligent Labeling Based on Fisher Information for Medical Image Segmentation Using Deep Learning. IEEE Transactions on Medical Imaging, 2019, 38, 2642-2653.	5.4	32
74	Impacting development in infants with tuberous sclerosis complex: Multidisciplinary research collaboration American Psychologist, 2019, 74, 356-367.	3.8	9
75	Deep Plug-and-Play Prior for Parallel MRI Reconstruction. , 2019, , .		8
76	Early white matter development is abnormal in tuberous sclerosis complex patients who develop autism spectrum disorder. Journal of Neurodevelopmental Disorders, 2019, 11, 36.	1.5	32
77	Fetal Echoplanar Imaging. Topics in Magnetic Resonance Imaging, 2019, 28, 245-254.	0.7	8
78	Fetal brain growth portrayed by a spatiotemporal diffusion tensor MRI atlas computed from in utero images. NeuroImage, 2019, 185, 593-608.	2.1	81
79	A registration method for improving quantitative assessment in probabilistic diffusion tractography. NeuroImage, 2019, 189, 288-306.	2.1	9
80	Motionâ€robust diffusion compartment imaging using simultaneous multiâ€slice acquisition. Magnetic Resonance in Medicine, 2019, 81, 3314-3329.	1.9	7
81	Asymmetric Loss Functions and Deep Densely-Connected Networks for Highly-Imbalanced Medical Image Segmentation: Application to Multiple Sclerosis Lesion Detection. IEEE Access, 2019, 7, 1721-1735.	2.6	120
82	Curved planar reformatting and convolutional neural networkâ€based segmentation of the small bowel for visualization and quantitative assessment of pediatric Crohn's disease from MRI. Journal of Magnetic Resonance Imaging, 2019, 49, 1565-1576.	1.9	20
83	Longitudinal Effects of Everolimus on White Matter Diffusion in Tuberous Sclerosis Complex. Pediatric Neurology, 2019, 90, 24-30.	1.0	21
84	Early-Emerging Sulcal Patterns Are Atypical in Fetuses with Congenital Heart Disease. Cerebral Cortex, 2019, 29, 3605-3616.	1.6	40
85	Volumetric Analysis of the Basal Ganglia and Cerebellar Structures in Patients with Phelan-McDermid Syndrome. Pediatric Neurology, 2019, 90, 37-43.	1.0	19
86	Towards microstructure fingerprinting: Estimation of tissue properties from a dictionary of Monte Carlo diffusion MRI simulations. NeuroImage, 2019, 184, 964-980.	2.1	38
87	Isotropic MRI Super-Resolution Reconstruction with Multi-scale Gradient Field Prior. Lecture Notes in Computer Science, 2019, 11766, 3-11.	1.0	11
88	Biomechanical Modelling of the Brain for Neuronavigation in Epilepsy Surgery. Biological and Medical Physics Series, 2019, , 165-180.	0.3	0
89	Non-learning based deep parallel MRI reconstruction (NLDpMRI). , 2019, , .		3
90	Corpus Callosum White Matter Diffusivity Reflects Cumulative Neurological Comorbidity in Tuberous Sclerosis Complex. Cerebral Cortex, 2018, 28, 3665-3672.	1.6	25

#	Article	IF	CITATIONS
91	Cerebellar volume as an imaging marker of development in infants with tuberous sclerosis complex. Neurology, 2018, 90, e1493-e1500.	1.5	9
92	Fetal Neuropathology in Zika Virus-Infected Pregnant Female Rhesus Monkeys. Cell, 2018, 173, 1111-1122.e10.	13.5	104
93	Presurgical language fMRI: Clinical practices and patient outcomes in epilepsy surgical planning. Human Brain Mapping, 2018, 39, 2777-2785.	1.9	41
94	Assessing the validity of the approximation of diffusionâ€weightedâ€MRI signals from crossing fascicles by sums of signals from single fascicles. Magnetic Resonance in Medicine, 2018, 79, 2332-2345.	1.9	18
95	Reproducibility of Brain MRI Segmentation Algorithms: Empirical Comparison of Local MAP PSTAPLE, FreeSurfer, and FSLâ€FIRST. Journal of Neuroimaging, 2018, 28, 162-172.	1.0	43
96	Missing Slice Recovery for Tensors Using a Low-Rank Model in Embedded Space. , 2018, , .		60
97	A Comparison of Point and Complete Electrode Models in a Finite Difference Model of Invasive Electrode Measurements. , 2018, 2018, 4677-4680.		2
98	Objective Evaluation of Multiple Sclerosis Lesion Segmentation using a Data Management and Processing Infrastructure. Scientific Reports, 2018, 8, 13650.	1.6	171
99	Active Deep Learning with Fisher Information for Patch-Wise Semantic Segmentation. Lecture Notes in Computer Science, 2018, 11045, 83-91.	1.0	19
100	Tract-Specific Group Analysis in Fetal Cohorts Using in utero Diffusion Tensor Imaging. Lecture Notes in Computer Science, 2018, 11072, 28-35.	1.0	3
101	Real-time automatic fetal brain extraction in fetal MRI by deep learning. , 2018, , .		50
102	Presurgical language fMRI: Technical practices in epilepsy surgical planning. Human Brain Mapping, 2018, 39, 4032-4042.	1.9	38
103	Automatic renal segmentation in DCE-MRI using convolutional neural networks. , 2018, 2018, 1534-1537.		32
104	Multi-compartment model of brain tissues from T2 relaxometry MRI using gamma distribution. , 2018, , .		4
105	Semi-automated Extraction of Crohns Disease MR Imaging Markers Using a 3D Residual CNN with Distance Prior. Lecture Notes in Computer Science, 2018, 11045, 218-226.	1.0	6
106	Differential Rates of Perinatal Maturation of Human Primary and Nonprimary Auditory Cortex. ENeuro, 2018, 5, ENEURO.0380-17.2017.	0.9	29
107	A Bayes Hilbert Space for Compartment Model Computing in Diffusion MRI. Lecture Notes in Computer Science, 2018, , 72-80.	1.0	0
108	Identification of Gadolinium Contrast Enhanced Regions in MS Lesions Using Brain Tissue Microstructure Information Obtained from Diffusion and T2 Relaxometry MRI. Lecture Notes in Computer Science, 2018, , 63-71.	1.0	1

#	Article	IF	CITATIONS
109	Longitudinal multiple sclerosis lesion segmentation: Resource and challenge. NeuroImage, 2017, 148, 77-102.	2.1	215
110	Block-Matching Distortion Correction of Echo-Planar Images With Opposite Phase Encoding Directions. IEEE Transactions on Medical Imaging, 2017, 36, 1106-1115.	5.4	26
111	A New Sparse Representation Framework for Reconstruction of an Isotropic High Spatial Resolution MR Volume From Orthogonal Anisotropic Resolution Scans. IEEE Transactions on Medical Imaging, 2017, 36, 1182-1193.	5.4	34
112	Reduced thalamic volume in patients with Electrical Status Epilepticus in Sleep. Epilepsy Research, 2017, 130, 74-80.	0.8	20
113	Heavy Prenatal Alcohol Exposure is Related to Smaller Corpus Callosum in Newborn <scp>MRI</scp> Scans. Alcoholism: Clinical and Experimental Research, 2017, 41, 965-975.	1.4	62
114	Automated template-based brain localization and extraction for fetal brain MRI reconstruction. NeuroImage, 2017, 155, 460-472.	2.1	31
115	Temporal slice registration and robust diffusion-tensor reconstruction for improved fetal brain structural connectivity analysis. NeuroImage, 2017, 156, 475-488.	2.1	54
116	Motion-robust parameter estimation in abdominal diffusion-weighted MRI by simultaneous image registration and model estimation. Medical Image Analysis, 2017, 39, 124-132.	7.0	20
117	Diffusion MRI microstructure models with in vivo human brain Connectome data: results from a multiâ€group comparison. NMR in Biomedicine, 2017, 30, e3734.	1.6	33
118	A normative spatiotemporal MRI atlas of the fetal brain for automatic segmentation and analysis of early brain growth. Scientific Reports, 2017, 7, 476.	1.6	217
119	Investigating the maturation of microstructure and radial orientation in the preterm human cortex with diffusion MRI. NeuroImage, 2017, 162, 65-72.	2.1	23
120	Presentation and Diagnosis of Tuberous Sclerosis Complex in Infants. Pediatrics, 2017, 140, .	1.0	90
121	White Matter Volume Predicts Language Development in Congenital Heart Disease. Journal of Pediatrics, 2017, 181, 42-48.e2.	0.9	52
122	A new neonatal cortical and subcortical brain atlas: the Melbourne Children's Regional Infant Brain (M-CRIB) atlas. NeuroImage, 2017, 147, 841-851.	2.1	74
123	Both 3-T dGEMRIC and Acetabular-Femoral T2 Difference May Detect Cartilage Damage at the Chondrolabral Junction. Clinical Orthopaedics and Related Research, 2017, 475, 1058-1065.	0.7	17
124	Dynamic Electrical Source Imaging (DESI) of Seizures and Interictal Epileptic Discharges Without Ensemble Averaging. IEEE Transactions on Medical Imaging, 2017, 36, 98-110.	5.4	5
125	Active delineation of Meyer's loop using oriented priors through MAGNEtic tractography (MAGNET). Human Brain Mapping, 2017, 38, 509-527.	1.9	42
126	Localization of stereo-electroencephalography signals using a finite difference complete electrode model. , 2017, 2017, 3600-3603.		3

#	Article	IF	CITATIONS
127	Decoupling Axial and Radial Tissue Heterogeneity in Diffusion Compartment Imaging. Lecture Notes in Computer Science, 2017, , 440-452.	1.0	3
128	Motion-Robust Spatially Constrained Parameter Estimation in Renal Diffusion-Weighted MRI by 3D Motion Tracking and Correction of Sequential Slices. Lecture Notes in Computer Science, 2017, 10555, 75-85.	1.0	3
129	Fetal lung apparent diffusion coefficient measurement using diffusion-weighted MRI at 3 Tesla: Correlation with gestational age. Journal of Magnetic Resonance Imaging, 2016, 44, 1650-1655.	1.9	14
130	Fast myelin water fraction estimation using 2D multislice <scp>CPMG</scp> . Magnetic Resonance in Medicine, 2016, 76, 1301-1313.	1.9	18
131	Hippocampal Formation Maldevelopment and Sudden Unexpected Death across the Pediatric Age Spectrum. Journal of Neuropathology and Experimental Neurology, 2016, 75, 981-997.	0.9	42
132	Evaluation of motion and its effect on brain magnetic resonance image quality in children. Pediatric Radiology, 2016, 46, 1728-1735.	1.1	35
133	Evaluation of numerical techniques for solving the current injection problem in biological tissues. , 2016, 2016, 876-880.		7
134	Extensions to a manifold learning framework for time-series analysis on dynamic manifolds in bioelectric signals. Physical Review E, 2016, 93, 042218.	0.8	23
135	Motion-Robust Reconstruction Based on Simultaneous Multi-slice Registration for Diffusion-Weighted MRI of Moving Subjects. Lecture Notes in Computer Science, 2016, 9902, 544-552.	1.0	8
136	Characterizing brain tissue by assessment of the distribution of anisotropic microstructural environments in diffusion ompartment imaging (DIAMOND). Magnetic Resonance in Medicine, 2016, 76, 963-977.	1.9	90
137	3D Superâ€Resolution Motionâ€Corrected MRI: Validation of Fetal Posterior Fossa Measurements. Journal of Neuroimaging, 2016, 26, 539-544.	1.0	15
138	Motion-Robust Diffusion-Weighted Brain MRI Reconstruction Through Slice-Level Registration-Based Motion Tracking. IEEE Transactions on Medical Imaging, 2016, 35, 2258-2269.	5.4	30
139	Spatially-constrained probability distribution model of incoherent motion (SPIM) for abdominal diffusion-weighted MRI. Medical Image Analysis, 2016, 32, 173-183.	7.0	17
140	Altered Structural Brain Networks in Tuberous Sclerosis Complex. Cerebral Cortex, 2016, 26, 2046-2058.	1.6	36
141	Single Anisotropic 3-D MR Image Upsampling via Overcomplete Dictionary Trained From In-Plane High Resolution Slices. IEEE Journal of Biomedical and Health Informatics, 2016, 20, 1552-1561.	3.9	27
142	Planar dGEMRIC Maps May Aid Imaging Assessment of Cartilage Damage in Femoroacetabular Impingement. Clinical Orthopaedics and Related Research, 2016, 474, 467-478.	0.7	21
143	Comprehensive Maximum Likelihood Estimation of Diffusion Compartment Models Towards Reliable Mapping of Brain Microstructure. Lecture Notes in Computer Science, 2016, , 622-630.	1.0	4
144	Improved fidelity of brain microstructure mapping from single-shell diffusion MRI. Medical Image Analysis, 2015, 26, 268-286.	7.0	15

#	Article	IF	CITATIONS
145	Superâ€resolution reconstruction in frequency, image, and wavelet domains to reduce throughâ€plane partial voluming in MRI. Medical Physics, 2015, 42, 6919-6932.	1.6	23
146	Normative biometrics for fetal ocular growth using volumetric MRI reconstruction. Prenatal Diagnosis, 2015, 35, 400-408.	1.1	22
147	Symmetric block-matching registration for the distortion correction of Echo-Planar images. , 2015, , .		0
148	A Model of Population and Subject (MOPS) Intensities With Application to Multiple Sclerosis Lesion Segmentation. IEEE Transactions on Medical Imaging, 2015, 34, 1349-1361.	5.4	55
149	Increased Brain Perfusion Persists over the First Month of Life in Term Asphyxiated Newborns Treated with Hypothermia: Does it Reflect Activated Angiogenesis?. Translational Stroke Research, 2015, 6, 224-233.	2.3	19
150	Structural and diffusion weighted MRI registration for biomarker fusion in Crohn's disease diagnosis. , 2015, , .		1
151	Optimized magnetic resonance diffusion protocol for ex-vivo whole human brain imaging with a clinical scanner. Proceedings of SPIE, 2015, , .	0.8	1
152	Tubers are neither static nor discrete. Neurology, 2015, 85, 1536-1545.	1.5	28
153	Combined delay and graph embedding of epileptic discharges in EEG reveals complex and recurrent nonlinear dynamics. , 2015, 2015, 347-350.		10
154	Spatially constrained incoherent motion method improves diffusionâ€weighted MRI signal decay analysis in the liver and spleen. Medical Physics, 2015, 42, 1895-1903.	1.6	21
155	Brain Perfusion Is Increased at Term in the White Matter of Very Preterm Newborns and Newborns with Congenital Heart Disease: Does this Reflect Activated Angiogenesis?. Neuropediatrics, 2015, 46, 344-351.	0.3	13
156	Motion Compensated Abdominal Diffusion Weighted MRI by Simultaneous Image Registration and Model Estimation (SIR-ME). Lecture Notes in Computer Science, 2015, 9351, 501-509.	1.0	5
157	Optimal MAP Parameters Estimation in STAPLE Using Local Intensity Similarity Information. IEEE Journal of Biomedical and Health Informatics, 2015, 19, 1589-1597.	3.9	4
158	A template-to-slice block matching approach for automatic localization of brain in fetal MRI. , 2015, , .		10
159	Multi-session complex averaging for high resolution high SNR 3T MR visualization of ex vivo hippocampus and insula. Proceedings of SPIE, 2015, , .	0.8	0
160	A Framework for the Analysis of Diffusion Compartment Imaging (DCI). Mathematics and Visualization, 2015, , 271-297.	0.4	2
161	Accelerated High Spatial Resolution Diffusion-Weighted Imaging. Lecture Notes in Computer Science, 2015, 24, 69-81.	1.0	7
162	Analytic Quantification of Bias and Variance ofÂCoil Sensitivity Profile Estimators for Improved Image Reconstruction in MRI. Lecture Notes in Computer Science, 2015, 9350, 684-691.	1.0	3

#	Article	IF	CITATIONS
163	MR Microscopy for 3D Identification of Cortical Tubers, White Matter "Microtubers―and Radial Migration Lines in Ex Vivo Pediatric TSC with Epilepsy. FASEB Journal, 2015, 29, .	0.2	0
164	Localization of the Epileptogenic Foci in Tuberous Sclerosis Complex: A Pediatric Case Report. Frontiers in Human Neuroscience, 2014, 8, 175.	1.0	26
165	Construction of a Deformable Spatiotemporal MRI Atlas of the Fetal Brain: Evaluation of Similarity Metrics and Deformation Models. Lecture Notes in Computer Science, 2014, 17, 292-299.	1.0	32
166	More accurate neuronavigation data provided by biomechanical modeling instead of rigid registration. Journal of Neurosurgery, 2014, 120, 1477-1483.	0.9	37
167	Optimization of tractography of the optic radiations. Human Brain Mapping, 2014, 35, 683-697.	1.9	47
168	Passive fMRI mapping of language function for pediatric epilepsy surgical planning: Validation using Wada, ECS, and FMAER. Epilepsy Research, 2014, 108, 1874-1888.	0.8	30
169	The anatomy and art of writing a successful grant application: a practical step-by-step approach. Pediatric Radiology, 2014, 44, 1512-1517.	1.1	16
170	Electrode localization for planning surgical resection of the epileptogenic zone in pediatric epilepsy. International Journal of Computer Assisted Radiology and Surgery, 2014, 9, 91-105.	1.7	32
171	A collaborative resource to build consensus for automated left ventricular segmentation of cardiac MR images. Medical Image Analysis, 2014, 18, 50-62.	7.0	143
172	Regional white matter microstructure in very preterm infants: Predictors and 7 year outcomes. Cortex, 2014, 52, 60-74.	1.1	101
173	A Mathematical Framework for the Registration and Analysis of Multi-Fascicle Models for Population Studies of the Brain Microstructure. IEEE Transactions on Medical Imaging, 2014, 33, 504-517.	5.4	33
174	Three-dimensional hip cartilage quality assessment of morphology and dGEMRIC by planar maps and automated segmentation. Osteoarthritis and Cartilage, 2014, 22, 1511-1515.	0.6	21
175	Voxel-Based Dipole Orientation Constraints for Distributed Current Estimation. IEEE Transactions on Biomedical Engineering, 2014, 61, 2028-2040.	2.5	6
176	A Logarithmic Opinion Pool Based STAPLE Algorithm for the Fusion of Segmentations With Associated Reliability Weights. IEEE Transactions on Medical Imaging, 2014, 33, 1997-2009.	5.4	52
177	Near-infrared spectroscopy versus magnetic resonance imaging to study brain perfusion in newborns with hypoxic–ischemic encephalopathy treated with hypothermia. NeuroImage, 2014, 85, 287-293.	2.1	93
178	Fetal MRI: A technical update with educational aspirations. Concepts in Magnetic Resonance Part A: Bridging Education and Research, 2014, 43, 237-266.	0.2	78
179	A Fully Bayesian Inference Framework for Population Studies of the Brain Microstructure. Lecture Notes in Computer Science, 2014, 17, 25-32.	1.0	4
180	T 2-Relaxometry for Myelin Water Fraction Extraction Using Wald Distribution and Extended Phase Graph. Lecture Notes in Computer Science, 2014, 17, 145-152.	1.0	9

#	Article	IF	CITATIONS
181	Optimal MAP Parameters Estimation in STAPLE - Learning from Performance Parameters versus Image Similarity Information. Lecture Notes in Computer Science, 2014, , 174-181.	1.0	2
182	Spatially-Constrained Probability Distribution Model of Incoherent Motion (SPIM) in Diffusion Weighted MRI Signals of Crohn's Disease. Lecture Notes in Computer Science, 2014, , 117-127.	1.0	4
183	Four Neuroimaging Questions that P-Values Cannot Answer (and Bayesian Analysis Can). Lecture Notes in Computer Science, 2014, , 95-106.	1.0	0
184	Magnetic Resonance Imaging of Pediatric Lung Parenchyma, Airways, Vasculature, Ventilation, and Perfusion. Radiologic Clinics of North America, 2013, 51, 555-582.	0.9	30
185	School-age effects of the newborn individualized developmental care and assessment program for preterm infants with intrauterine growth restriction: preliminary findings. BMC Pediatrics, 2013, 13, 25.	0.7	48
186	Brain functional networks in syndromic and non-syndromic autism: a graph theoretical study of EEG connectivity. BMC Medicine, 2013, 11, 54.	2.3	149
187	Biomechanical Model as a Registration Tool for Image-Guided Neurosurgery: Evaluation Against BSpline Registration. Annals of Biomedical Engineering, 2013, 41, 2409-2425.	1.3	34
188	Simultaneous Truth and Performance Level Estimation Through Fusion of Probabilistic Segmentations. IEEE Transactions on Medical Imaging, 2013, 32, 1840-1852.	5.4	64
189	Reliable estimation of incoherent motion parametric maps from diffusion-weighted MRI using fusion bootstrap moves. Medical Image Analysis, 2013, 17, 325-336.	7.0	62
190	Cortical Graph Smoothing: A Novel Method for Exploiting DWI-Derived Anatomical Brain Connectivity to Improve EEG Source Estimation. IEEE Transactions on Medical Imaging, 2013, 32, 1952-1963.	5.4	21
191	Hippocampal shape variations at term equivalent age in very preterm infants compared with term controls: Perinatal predictors and functional significance at age 7. NeuroImage, 2013, 70, 278-287.	2.1	57
192	A Magnetic Resonance Imaging Study of Cerebellar Volume in Tuberous Sclerosis Complex. Pediatric Neurology, 2013, 48, 105-110.	1.0	25
193	Characterization of fast and slow diffusion from diffusionâ€weighted MRI of pediatric Crohn's disease. Journal of Magnetic Resonance Imaging, 2013, 37, 156-163.	1.9	40
194	Diffusion tensor imaging and related techniques in tuberous sclerosis complex: review and future directions. Future Neurology, 2013, 8, 583-597.	0.9	40
195	Impaired Language Pathways in Tuberous Sclerosis Complex Patients with Autism Spectrum Disorders. Cerebral Cortex, 2013, 23, 1526-1532.	1.6	72
196	Perfusion Imaging of Focal Cortical Dysplasia Using Arterial Spin Labeling. Journal of Child Neurology, 2013, 28, 1474-1482.	0.7	37
197	Automatic delineation of white matter fascicles by localization based upon anatomical spatial relationships. , 2013, , .		1
108	Intra-operative Update of Neuro-images: Comparison of Performance of Image Warping Using		1

Patient-Specific Biomechanical Model and BSpline Image Registration. , 2013, , 127-141. 198

1

#	Article	IF	CITATIONS
199	Objective Evaluation of Accuracy of Intra-Operative Neuroimage Registration. , 2013, , 87-99.		7
200	Reliable Selection of the Number of Fascicles in Diffusion Images by Estimation of the Generalization Error. Lecture Notes in Computer Science, 2013, 23, 742-753.	1.0	14
201	Characterizing the Distribution of Anisotropic MicrO-structural eNvironments with Diffusion-Weighted Imaging (DIAMOND). Lecture Notes in Computer Science, 2013, 16, 518-526.	1.0	17
202	Estimation of a Multi-fascicle Model from Single B-Value Data with a Population-Informed Prior. Lecture Notes in Computer Science, 2013, 16, 695-702.	1.0	9
203	Spatially Constrained Incoherent Motion (SCIM) Model Improves Quantitative Diffusion-Weighted MRI Analysis of Crohn's Disease Patients. Lecture Notes in Computer Science, 2013, , 11-19.	1.0	1
204	Improved Multi B-Value Diffusion-Weighted MRI of the Body by Simultaneous Model Estimation and Image Reconstruction (SMEIR). Lecture Notes in Computer Science, 2013, 16, 1-8.	1.0	5
205	Serial FEM/XFEM-Based Update of Preoperative Brain Images Using Intraoperative MRI. International Journal of Biomedical Imaging, 2012, 2012, 1-17.	3.0	13
206	A generalized correlation coefficient: Application to DTI and multi-fiber DTI. , 2012, , .		5
207	Whole brain group network analysis using network bias and variance parameters. , 2012, 2012, 1511-1514.		1
208	Polyaffine parametrization of image registration based on geodesic flows. , 2012, , .		2
209	Retrospective local artefacts detection in diffusion-weighted images using the Random Sample Consensus (RANSAC) paradigm. , 2012, , .		3
210	Estimating A Reference Standard Segmentation With Spatially Varying Performance Parameters: Local MAP STAPLE. IEEE Transactions on Medical Imaging, 2012, 31, 1593-1606.	5.4	64
211	Loss of White Matter Microstructural Integrity Is Associated with Adverse Neurological Outcome in Tuberous Sclerosis Complex. Academic Radiology, 2012, 19, 17-25.	1.3	111
212	Super-resolution reconstruction of diffusion-weighted images from distortion compensated orthogonal anisotropic acquisitions. , 2012, 2012, 249-254.		5
213	Interpolating multi-fiber models by Gaussian mixture simplification. , 2012, , .		6
214	Automated delineation of white matter fiber tracts with a multiple region-of-interest approach. NeuroImage, 2012, 59, 3690-3700.	2.1	49
215	Corpus callosum alterations in very preterm infants: Perinatal correlates and 2year neurodevelopmental outcomes. NeuroImage, 2012, 59, 3571-3581.	2.1	98
216	Multi-atlas multi-shape segmentation of fetal brain MRI for volumetric and morphometric analysis of ventriculomegaly. NeuroImage, 2012, 60, 1819-1831.	2.1	74

#	Article	IF	CITATIONS
217	Anisotropic partial volume CSF modeling for EEG source localization. NeuroImage, 2012, 62, 2161-2170.	2.1	21
218	Super-resolution reconstruction to increase the spatial resolution of diffusion weighted images from orthogonal anisotropic acquisitions. Medical Image Analysis, 2012, 16, 1465-1476.	7.0	106
219	<i>In vivo</i> assessment of optimal <i>b</i> â€value range for perfusionâ€insensitive apparent diffusion coefficient imaging. Medical Physics, 2012, 39, 4832-4839.	1.6	42
220	New Insights in Perinatal Arterial Ischemic Stroke by Assessing Brain Perfusion. Translational Stroke Research, 2012, 3, 255-262.	2.3	24
221	Optimizing Hippocampal Segmentation in Infants Utilizing MRI Post-Acquisition Processing. Neuroinformatics, 2012, 10, 173-180.	1.5	17
222	Quantitative in vivo MRI measurement of cortical development in the fetus. Brain Structure and Function, 2012, 217, 127-139.	1.2	140
223	Performing Brain Image Warping Using the Deformation Field Predicted by a Biomechanical Model. , 2012, , 89-96.		5
224	Neuroimage as a Biomechanical Model: Toward New Computational Biomechanics of the Brain. , 2012, , 19-28.		2
225	Left Ventricular Segmentation Challenge from Cardiac MRI: A Collation Study. Lecture Notes in Computer Science, 2012, , 88-97.	1.0	26
226	Abdominal Images Non-rigid Registration Using Local-Affine Diffeomorphic Demons. Lecture Notes in Computer Science, 2012, , 116-124.	1.0	2
227	Reliable Assessment of Perfusivity and Diffusivity from Diffusion Imaging of the Body. Lecture Notes in Computer Science, 2012, 15, 1-9.	1.0	10
228	Estimation of the Prior Distribution of Ground Truth in the STAPLE Algorithm: An Empirical Bayesian Approach. Lecture Notes in Computer Science, 2012, 15, 593-600.	1.0	4
229	Parametric Representation of Multiple White Matter Fascicles from Cube and Sphere Diffusion MRI. PLoS ONE, 2012, 7, e48232.	1.1	65
230	School age effects of the Newborn Individualized Developmental Care and Assessment Program for medically low-risk preterm infants: Preliminary findings. Journal of Clinical Neonatology, 2012, 1, 184.	0.1	14
231	Registration and Analysis of White Matter Group Differences with a Multi-fiber Model. Lecture Notes in Computer Science, 2012, 15, 313-320.	1.0	12
232	Cortical brain structures segmentation using constrained optimization and intensity coupling. , 2011, , \cdot		0
233	On the Effects of Model Complexity in Computing Brain Deformation for Image-Guided Neurosurgery. , 2011, , 51-61.		1
234	Characterization of the corpus callosum in very preterm and full-term infants utilizing MRI. NeuroImage, 2011, 55, 479-490.	2.1	108

#	ARTICLE	IF	CITATIONS
235	A new classifier feature space for an improved Multiple Sclerosis lesion segmentation. , 2011, , .		8
236	Accelerating Image Registration With the Johnson–Lindenstrauss Lemma: Application to Imaging 3-D Neural Ultrastructure With Electron Microscopy. IEEE Transactions on Medical Imaging, 2011, 30, 1427-1438.	5.4	9
237	Fetal brain volumetry through MRI volumetric reconstruction and segmentation. International Journal of Computer Assisted Radiology and Surgery, 2011, 6, 329-339.	1.7	62
238	Segmentations of MRI images of the female pelvic floor: A study of inter―and intra―eader reliability. Journal of Magnetic Resonance Imaging, 2011, 33, 684-691.	1.9	47
239	3D XFEM-based modeling of retraction for preoperative image update. Computer Aided Surgery, 2011, 16, 121-134.	1.8	15
240	Automated detection of white matter fiber bundles. , 2011, , .		0
241	Motion-robust MRI through real-time motion tracking and retrospective super-resolution volume reconstruction. , 2011, 2011, 5722-5.		13
242	Anisotropic equivalent conductivity tensors for bioelectric modeling of partial volume effects in cerebrospinal fluid spaces. , 2011, , .		0
243	Early versus late MRI in asphyxiated newborns treated with hypothermia. Archives of Disease in Childhood: Fetal and Neonatal Edition, 2011, 96, F36-F44.	1.4	59
244	On the accuracy of unwarping techniques for the correction of susceptibility-induced geometric distortion in magnetic resonance Echo-planar images. , 2011, 2011, 6997-7000.		14
245	Demons registration with local affine adaptive regularization: application to registration of abdominal structures. , 2011, , .		11
246	SoftSTAPLE: Truth and performance-level estimation from probabilistic segmentations. , 2011, , .		3
247	Toward an accurate multi-fiber assessment strategy for clinical practice. , 2011, , .		7
248	Learning Likelihoods for Labeling (L3): A General Multi-Classifier Segmentation Algorithm. Lecture Notes in Computer Science, 2011, 14, 322-329.	1.0	19
249	Super-Resolution in Diffusion-Weighted Imaging. Lecture Notes in Computer Science, 2011, 14, 124-132.	1.0	15
250	Spatially Adaptive Log-Euclidean Polyaffine Registration Based on Sparse Matches. Lecture Notes in Computer Science, 2011, 14, 590-597.	1.0	7
251	Can induced hypothermia be assured during brain MRI in neonates with hypoxic-ischemic encephalopathy?. Pediatric Radiology, 2010, 40, 1950-1954.	1.1	28
252	Automatic Segmentation and Quantitative Analysis of the Articular Cartilages From Magnetic Resonance Images of the Knee. IEEE Transactions on Medical Imaging, 2010, 29, 55-64.	5.4	158

#	Article	IF	CITATIONS
253	Estimation of Inferential Uncertainty in Assessing Expert Segmentation Performance From STAPLE. IEEE Transactions on Medical Imaging, 2010, 29, 771-780.	5.4	28
254	Robust Super-Resolution Volume Reconstruction From Slice Acquisitions: Application to Fetal Brain MRI. IEEE Transactions on Medical Imaging, 2010, 29, 1739-1758.	5.4	275
255	Patient-specific non-linear finite element modelling for predicting soft organ deformation in real-time; Application to non-rigid neuroimage registration. Progress in Biophysics and Molecular Biology, 2010, 103, 292-303.	1.4	74
256	Enhanced FEM-based modeling of brain shift deformation in Image-Guided Neurosurgery. Journal of Computational and Applied Mathematics, 2010, 234, 2046-2053.	1.1	17
257	Measuring effects of latency in brain activity with fMRI. , 2010, , .		0
258	Why multiple b-values are required for multi-tensor models. evaluation with a constrained log-euclidean model. , 2010, , .		15
259	Morphological Characteristics of Brain Tumors Causing Seizures. Archives of Neurology, 2010, 67, 336-42.	4.9	139
260	Fetal Placental Thrombosis and Neonatal Implications. American Journal of Perinatology, 2010, 27, 251-256.	0.6	20
261	Diffusion Features of White Matter in Tuberous Sclerosis With Tractography. Pediatric Neurology, 2010, 42, 101-106.	1.0	59
262	Controllable spatio-temporal smoothness constraints for EEG source localization. , 2010, , .		0
263	Incorporating Priors on Expert Performance Parameters for Segmentation Validation and Label Fusion: A Maximum a Posteriori STAPLE. Lecture Notes in Computer Science, 2010, 13, 25-32.	1.0	32
264	Maximum A Posteriori Estimation of Isotropic High-Resolution Volumetric MRI from Orthogonal Thick-Slice Scans. Lecture Notes in Computer Science, 2010, 13, 109-116.	1.0	16
265	A data-driven approach to discovering common brain anatomy. , 2009, , .		0
266	Brain Development of the Preterm Neonate After Neonatal Hydrocortisone Treatment for Chronic Lung Disease. Pediatric Research, 2009, 66, 555-559.	1.1	58
267	2D XFEM-based modeling of retraction and successive resections for preoperative image update. Computer Aided Surgery, 2009, 14, 1-20.	1.8	13
268	A Continuous STAPLE for Scalar, Vector, and Tensor Images: An Application to DTI Analysis. IEEE Transactions on Medical Imaging, 2009, 28, 838-846.	5.4	31
269	MRâ€determined hippocampal asymmetry in fullâ€ŧerm and preterm neonates. Hippocampus, 2009, 19, 118-123.	. 0.9	55
270	Reproducibility of Laplacian Wall Thickness Measurements of the Gallbladder with Varying CT Slice Thickness. Journal of Signal Processing Systems, 2009, 55, 67-75.	1.4	3

#	Article	IF	CITATIONS
271	Standardized evaluation methodology and reference database for evaluating coronary artery centerline extraction algorithms. Medical Image Analysis, 2009, 13, 701-714.	7.0	295
272	Real-Time Prediction of Brain Shift Using Nonlinear Finite Element Algorithms. Lecture Notes in Computer Science, 2009, 12, 300-307.	1.0	28
273	Improved registration for large electron microscopy images. , 2009, , .		5
274	EEG source analysis of epileptiform activity using a 1Âmm anisotropic hexahedra finite element head model. NeuroImage, 2009, 44, 399-410.	2.1	145
275	Automatic segmentation of newborn brain MRI. NeuroImage, 2009, 47, 564-572.	2.1	185
276	Using Frankenstein's Creature Paradigm to Build a Patient Specific Atlas. Lecture Notes in Computer Science, 2009, 12, 993-1000.	1.0	27
277	Accelerating Feature Based Registration Using the Johnson-Lindenstrauss Lemma. Lecture Notes in Computer Science, 2009, 12, 632-639.	1.0	5
278	Estimation of Inferential Uncertainty in Assessing Expert Segmentation Performance from Staple. Lecture Notes in Computer Science, 2009, 21, 701-712.	1.0	1
279	A unified framework for clustering and quantitative analysis of white matter fiber tracts. Medical Image Analysis, 2008, 12, 191-202.	7.0	122
280	A quantitative assessment of approaches to mesh generation for surgical simulation. Engineering With Computers, 2008, 24, 417-430.	3.5	2
281	Neonate hippocampal volumes: Prematurity, perinatal predictors, and 2â€year outcome. Annals of Neurology, 2008, 63, 642-651.	2.8	142
282	Quantity and distribution of levator ani stretch during simulated vaginal childbirth. American Journal of Obstetrics and Gynecology, 2008, 199, 198.e1-198.e5.	0.7	96
283	A rhesus monkey reference label atlas for template driven segmentation. Journal of Medical Primatology, 2008, 37, 250-260.	0.3	6
284	An MRI study of age-related white and gray matter volume changes in the rhesus monkey. Neurobiology of Aging, 2008, 29, 1563-1575.	1.5	65
285	Comparison of the deformations of brain tissues caused by tumor in seizure and non-seizure patients. , 2008, , .		0
286	Primary cortical folding in the human newborn: an early marker of later functional development. Brain, 2008, 131, 2028-2041.	3.7	409
287	Volumetric MRI Study of Brain in Children With Intrauterine Exposure to Cocaine, Alcohol, Tobacco, and Marijuana. Pediatrics, 2008, 121, 741-750.	1.0	140
288	Intrauterine Growth Restriction Affects the Preterm Infant's Hippocampus. Pediatric Research, 2008, 63, 438-443.	1.1	187

#	Article	IF	CITATIONS
289	COMPENSATION OF GEOMETRIC DISTORTION EFFECTS ON INTRAOPERATIVE MAGNETIC RESONANCE IMAGING FOR ENHANCED VISUALIZATION IN IMAGE-GUIDED NEUROSURGERY. Operative Neurosurgery, 2008, 62, 209-216.	0.4	17
290	Validation of image segmentation by estimating rater bias and variance. Philosophical Transactions Series A, Mathematical, Physical, and Engineering Sciences, 2008, 366, 2361-2375.	1.6	48
291	Detection of DTI White Matter Abnormalities in Multiple Sclerosis Patients. Lecture Notes in Computer Science, 2008, 11, 975-982.	1.0	21
292	EEG to MRI Registration Based on Global and Local Similarities of MRI Intensity Distributions. Lecture Notes in Computer Science, 2008, 11, 762-770.	1.0	4
293	Evaluation of Brain MRI Alignment with the Robust Hausdorff Distance Measures. Lecture Notes in Computer Science, 2008, , 594-603.	1.0	22
294	Magnetic Resonance Image-Guided Neurosurgeryâ^—â^—Reproduced from the first edition, Handbook of Neuro-Oncology Neuroimaging, ed. F. Jolesz and H. Newton, Academic Press, 2007 , 2008, , 205-215.		1
295	Magnetic Resonance Image Guided Neurosurgery. , 2008, , 171-180.		0
296	3D Segmentation in the Clinic: A Grand Challenge II: MS lesion segmentation. , 2008, , .		56
297	Alignment of Large Image Series Using Cubic B-Splines Tessellation: Application to Transmission Electron Microscopy Data. , 2007, 10, 710-717.		5
298	Automatic Segmentation of Articular Cartilage in Magnetic Resonance Images of the Knee. , 2007, 10, 186-194.		19
299	Perinatal risk factors altering regional brain structure in the preterm infant. Brain, 2007, 130, 667-677.	3.7	274
300	AUTOMATIC SEGMENTATION OF THE BONES FROM MR IMAGES OF THE KNEE. , 2007, , .		4
301	Non-rigid alignment of pre-operative MRI, fMRI, and DT-MRI with intra-operative MRI for enhanced visualization and navigation in image-guided neurosurgery. NeuroImage, 2007, 35, 609-624.	2.1	180
302	Displacement of brain regions in preterm infants with non-synostotic dolichocephaly investigated by MRI. NeuroImage, 2007, 36, 1074-1085.	2.1	30
303	Comparison of fiber tracts derived from in-vivo DTI tractography with 3D histological neural tract tracer reconstruction on a macaque brain. NeuroImage, 2007, 37, 530-538.	2.1	216
304	A Validation Framework for Brain Tumor Segmentation. Academic Radiology, 2007, 14, 1242-1251.	1.3	83
305	Automatic segmentation of the bone and extraction of the bone–cartilage interface from magnetic resonance images of the knee. Physics in Medicine and Biology, 2007, 52, 1617-1631.	1.6	94
306	Estimation of the deformations induced by articulated bodies: Registration of the spinal column. Biomedical Signal Processing and Control, 2007, 2, 16-24.	3.5	16

#	Article	IF	CITATIONS
307	A fuzzy system for helping medical diagnosis of malformations of cortical development. Journal of Biomedical Informatics, 2007, 40, 221-235.	2.5	47
308	Racial differences in pelvic floor muscle thickness in asymptomatic nulliparas as seen on magnetic resonance imaging–based three-dimensional color thickness mapping. American Journal of Obstetrics and Gynecology, 2007, 197, 625.e1-625.e4.	0.7	8
309	Patient-specific model of brain deformation: Application to medical image registration. Journal of Biomechanics, 2007, 40, 919-929.	0.9	189
310	Probabilistic Clustering and Quantitative Analysis of White Matter Fiber Tracts. Lecture Notes in Computer Science, 2007, 20, 372-383.	1.0	31
311	Grid-Enabled Software Environment for Enhanced Dynamic Data-Driven Visualization and Navigation During Image-Guided Neurosurgery. Lecture Notes in Computer Science, 2007, , 980-987.	1.0	0
312	Guest Editorial Validation in Medical Image Processing. IEEE Transactions on Medical Imaging, 2006, 25, 1405-1409.	5.4	51
313	Toward Real-Time Image Guided Neurosurgery Using Distributed and Grid Computing. , 2006, , .		28
314	Automated segmentation of multiple sclerosis lesion subtypes with multichannel MRI. NeuroImage, 2006, 32, 1205-1215.	2.1	115
315	Integration of patient specific modeling and advanced image processing techniques for image-guided neurosurgery. , 2006, , .		9
316	XFEM-based modeling of successive resections for preoperative image updating. , 2006, 6141, 403.		2
317	Novel image processing techniques to better understand white matter disruption in multiple sclerosis. Autoimmunity Reviews, 2006, 5, 544-548.	2.5	5
318	Image-guided neurosurgery at Brigham and Women's Hospital. IEEE Engineering in Medicine and Biology Magazine, 2006, 25, 67-73.	1.1	34
319	Reduction in Cerebellar Volumes in Preterm Infants: Relationship to White Matter Injury and Neurodevelopment at Two Years of Age. Pediatric Research, 2006, 60, 97-102.	1.1	130
320	Imaging and visual analysisToward real-time image guided neurosurgery using distributed and grid computing. , 2006, , .		14
321	Reduced Occipital Regional Volumes at Term Predict Impaired Visual Function in Early Childhood in Very Low Birth Weight Infants. , 2006, 47, 3366.		41
322	A subdivision-based parametric deformable model for surface extraction and statistical shape modeling of the knee cartilages. , 2006, 6141, 622.		0
323	Regional Brain Development in Serial Magnetic Resonance Imaging of Low-Risk Preterm Infants. Pediatrics, 2006, 118, 23-33.	1.0	139
324	3D Histological Reconstruction of Fiber Tracts and Direct Comparison with Diffusion Tensor MRI Tractography. Lecture Notes in Computer Science, 2006, 9, 109-116.	1.0	14

#	Article	IF	CITATIONS
325	Highly Accurate Segmentation of Brain Tissue and Subcortical Gray Matter from Newborn MRI. Lecture Notes in Computer Science, 2006, 9, 199-206.	1.0	20
326	Validation of Image Segmentation by Estimating Rater Bias and Variance. Lecture Notes in Computer Science, 2006, 9, 839-847.	1.0	12
327	Incorporating Metric Flows and Sparse Jacobian Transformations in ITK. The Insight Journal, 2006, , .	0.2	1
328	Capturing intraoperative deformations: research experience at Brigham and Women's hospital. Medical Image Analysis, 2005, 9, 145-162.	7.0	75
329	Talairachâ€Based Parcellation of Neonatal Brain Magnetic Resonance Imaging Data: Validation of a New Approach. Journal of Neuroimaging, 2005, 15, 305-314.	1.0	4
330	Efficient multi-modal dense field non-rigid registration: alignment of histological and section images. Medical Image Analysis, 2005, 9, 538-546.	7.0	29
331	An EM algorithm for shape classification based on level sets. Medical Image Analysis, 2005, 9, 491-502.	7.0	34
332	Hybrid Formulation of the Model-Based Non-rigid Registration Problem to Improve Accuracy and Robustness. Lecture Notes in Computer Science, 2005, 8, 295-302.	1.0	2
333	Impaired Trophic Interactions Between the Cerebellum and the Cerebrum Among Preterm Infants. Pediatrics, 2005, 116, 844-850.	1.0	200
334	Reproducibility of Functional MR Imaging: Preliminary Results of Prospective Multi-institutional Study Performed by Biomedical Informatics Research Network. Radiology, 2005, 237, 781-789.	3.6	92
335	An In Vivo MRI Study of Prefrontal Cortical Complexity in First-Episode Psychosis. American Journal of Psychiatry, 2005, 162, 65-70.	4.0	40
336	Late Gestation Cerebellar Growth Is Rapid and Impeded by Premature Birth. Pediatrics, 2005, 115, 688-695.	1.0	353
337	Realistic simulation of the 3-D growth of brain tumors in MR images coupling diffusion with biomechanical deformation. IEEE Transactions on Medical Imaging, 2005, 24, 1334-1346.	5.4	299
338	Abnormal Cerebral Structure Is Present at Term in Premature Infants. Pediatrics, 2005, 115, 286-294.	1.0	775
339	Three-dimensional assessment of MR imaging-guided percutaneous cryotherapy using multi-performer repeated segmentations. Academic Radiology, 2005, 12, 444-450.	1.3	9
340	Robust nonrigid registration to capture brain shift from intraoperative MRI. IEEE Transactions on Medical Imaging, 2005, 24, 1417-1427.	5.4	214
341	Diffusion Tensor Magnetic Resonance Imaging in Multiple Sclerosis. Journal of Neuroimaging, 2005, 15, 68S-81S.	1.0	74
342	Non-rigid registration of a 3D ultrasound and a MR image data set of the female pelvic floor using a biomechanical model. BioMedical Engineering OnLine, 2005, 4, 19.	1.3	8

#	Article	IF	CITATIONS
343	Accrual of MRI white matter abnormalities in elderly with normal and impaired mobility. Journal of the Neurological Sciences, 2005, 232, 23-27.	0.3	70
344	Automated Atlas-Based Clustering of White Matter Fiber Tracts from DTMRI. Lecture Notes in Computer Science, 2005, 8, 188-195.	1.0	63
345	Combining Classifiers Using Their Receiver Operating Characteristics and Maximum Likelihood Estimation. Lecture Notes in Computer Science, 2005, 8, 506-514.	1.0	20
346	Brain Shift Computation Using a Fully Nonlinear Biomechanical Model. Lecture Notes in Computer Science, 2005, 8, 583-590.	1.0	49
347	3D Statistical Shape Models to Embed Spatial Relationship Information. Lecture Notes in Computer Science, 2005, , 51-60.	1.0	11
348	Spectral Clustering Algorithms for Ultrasound Image Segmentation. Lecture Notes in Computer Science, 2005, 8, 862-869.	1.0	14
349	Tetrahedral mesh generation for medical imaging. The Insight Journal, 2005, , .	0.2	6
350	Talairach-Based Parcellation of Neonatal Brain Magnetic Resonance Imaging Data: Validation of a New Approach. , 2005, 15, 305-314.		0
351	Early Alteration of Structural and Functional Brain Development in Premature Infants Born with Intrauterine Growth Restriction. Pediatric Research, 2004, 56, 132-138.	1.1	402
352	Three-Dimensional Assessment of MRI-Guided Percutaneous Cryotherapy of Liver Metastases. American Journal of Roentgenology, 2004, 183, 707-712.	1.0	44
353	Has your patient's multiple sclerosis lesion burden or brain atrophy actually changed?. Multiple Sclerosis Journal, 2004, 10, 402-406.	1.4	24
354	In Silico Tumor Growth: Application to Glioblastomas. Lecture Notes in Computer Science, 2004, , 337-345.	1.0	13
355	On Extended Finite Element Method (XFEM) for Modelling of Organ Deformations Associated with Surgical Cuts. Lecture Notes in Computer Science, 2004, , 134-143.	1.0	12
356	Levator ani thickness variations in symptomatic and asymptomatic women using magnetic resonance-based 3-dimensional color mapping. American Journal of Obstetrics and Gynecology, 2004, 191, 856-861.	0.7	87
357	A limited range of measures of 2-d ultrasound correlate with 3-d mri cerebral volumes in the premature infant at term. Ultrasound in Medicine and Biology, 2004, 30, 11-18.	0.7	25
358	Three validation metrics for automated probabilistic image segmentation of brain tumours. Statistics in Medicine, 2004, 23, 1259-1282.	0.8	96
359	Application of spherical harmonics derived space rotation invariant indices to the analysis of multiple sclerosis lesions' geometry by MRI. Magnetic Resonance Imaging, 2004, 22, 815-825.	1.0	3
360	Multi-subject Registration for Unbiased Statistical Atlas Construction. Lecture Notes in Computer Science, 2004, , 655-662.	1.0	23

#	Article	IF	CITATIONS
361	Statistical validation of image segmentation quality based on a spatial overlap index1. Academic Radiology, 2004, 11, 178-189.	1.3	1,363
362	Prefrontal cortical thickness in first-episode psychosis: a magnetic resonance imaging study. Biological Psychiatry, 2004, 55, 131-140.	0.7	73
363	Simultaneous Truth and Performance Level Estimation (STAPLE): An Algorithm for the Validation of Image Segmentation. IEEE Transactions on Medical Imaging, 2004, 23, 903-921.	5.4	1,604
364	Validation of 3D assessment of MR imaging-guided percutaneous cryotherapy of a soft-tissue metastasis. International Congress Series, 2004, 1268, 313-317.	0.2	0
365	Improved Watershed Transform for Medical Image Segmentation Using Prior Information. IEEE Transactions on Medical Imaging, 2004, 23, 447-458.	5.4	594
366	Modelling Surgical Cuts, Retractions, and Resections via Extended Finite Element Method. Lecture Notes in Computer Science, 2004, , 311-318.	1.0	14
367	Dense deformation field estimation for brain intraoperative images registration. , 2004, , .		1
368	Early Experience Alters Brain Function and Structure. Pediatrics, 2004, 113, 846-857.	1.0	735
369	Level Set Methods in an EM Framework for Shape Classification and Estimation. Lecture Notes in Computer Science, 2004, , 1-9.	1.0	4
370	Improved Non-rigid Registration of Prostate MRI. Lecture Notes in Computer Science, 2004, , 845-852.	1.0	12
371	Landmark-Guided Surface Matching and Volumetric Warping for Improved Prostate Biopsy Targeting and Guidance. Lecture Notes in Computer Science, 2004, , 853-861.	1.0	11
372	Automatic Optimization of Segmentation Algorithms Through Simultaneous Truth and Performance Level Estimation (STAPLE). Lecture Notes in Computer Science, 2004, , 274-282.	1.0	6
373	An Anisotropic Material Model for Image Guided Neurosurgery. Lecture Notes in Computer Science, 2004, , 267-275.	1.0	6
374	A Prospective Multi-institutional Study of the Reproducibility of fMRI: A Preliminary Report from the Biomedical Informatics Research Network. Lecture Notes in Computer Science, 2004, , 769-776.	1.0	3
375	Coupling Statistical Segmentation and PCA Shape Modeling. Lecture Notes in Computer Science, 2004, 3216, 151-159.	1.0	8
376	Tumor detection in the bladder wall with a measurement of abnormal thickness in CT scans. IEEE Transactions on Biomedical Engineering, 2003, 50, 383-390.	2.5	46
377	Statistical validation based on parametric receiver operating characteristic analysis of continuous classification data1. Academic Radiology, 2003, 10, 1359-1368.	1.3	29
378	An Efficient Algorithm for Multiple Sclerosis Lesion Segmentation from Brain MRI. Lecture Notes in Computer Science, 2003, , 542-551.	1.0	9

#	Article	IF	CITATIONS
379	Assessment of the impact of the removal of cerebrospinal fluid on cerebral tissue volumes by advanced volumetric 3D-MRI in posthaemorrhagic hydrocephalus in a premature infant. Journal of Neurology, Neurosurgery and Psychiatry, 2003, 74, 658-660.	0.9	22
380	Capturing Brain Deformation. Lecture Notes in Computer Science, 2003, , 203-217.	1.0	2
381	Diffusion Tensor and Functional MRI Fusion with Anatomical MRI for Image-Guided Neurosurgery. Lecture Notes in Computer Science, 2003, , 407-415.	1.0	24
382	Augmenting intraoperative MRI with preoperative fMRI and DTI by biomechanical simulation of brain deformation. , 2003, , .		1
383	A New Technique for Multi-modal 3D Image Registration. Lecture Notes in Computer Science, 2003, , 244-253.	1.0	0
384	Validation of Image Segmentation and Expert Quality with an Expectation-Maximization Algorithm. Lecture Notes in Computer Science, 2002, , 298-306.	1.0	57
385	Incorporating Non-rigid Registration into Expectation Maximization Algorithm to Segment MR Images. Lecture Notes in Computer Science, 2002, 2488, 564-571.	1.0	31
386	Quantitative MR Imaging Assessment of Prostate Gland Deformation before and During MR Imaging–Guided Brachytherapy. Academic Radiology, 2002, 9, 906-912.	1.3	51
387	Labeling the Brain Surface Using a Deformable Multiresolution Mesh. Lecture Notes in Computer Science, 2002, , 451-458.	1.0	13
388	TUMOR DETECTION BY VIRTUAL CYSTOSCOPY WITH COLOR MAPPING OF BLADDER WALL THICKNESS. Journal of Urology, 2002, 167, 559-562.	0.2	53
389	Advanced Nonrigid Registration Algorithms for Image Fusion. , 2002, , 661-690.		6
390	Quantitative analysis of MRI signal abnormalities of brain white matter with high reproducibility and accuracy. Journal of Magnetic Resonance Imaging, 2002, 15, 203-209.	1.9	118
391	Real-time registration of volumetric brain MRI by biomechanical simulation of deformation during image guided neurosurgery. Computing and Visualization in Science, 2002, 5, 3-11.	1.2	91
392	Serial registration of intraoperative MR images of the brain. Medical Image Analysis, 2002, 6, 337-359.	7.0	184
393	Nonrigid registration of 3D tensor medical data. Medical Image Analysis, 2002, 6, 143-161.	7.0	131
394	Statistical Validation of Automated Probabilistic Segmentation against Composite Latent Expert Ground Truth in MR Imaging of Brain Tumors. Lecture Notes in Computer Science, 2002, , 315-322.	1.0	6
395	TUMOR DETECTION BY VIRTUAL CYSTOSCOPY WITH COLOR MAPPING OF BLADDER WALL THICKNESS. Journal of Urology, 2002, 167, 559-562.	0.2	31
396	Evaluation of three-dimensional finite element-based deformable registration of pre- and intraoperative prostate imaging. Medical Physics, 2001, 28, 2551-2560.	1.6	201

#	Article	IF	CITATIONS
397	Automated Segmentation of MR Images of Brain Tumors. Radiology, 2001, 218, 586-591.	3.6	432
398	Registration of 3-d intraoperative MR images of the brain using a finite-element biomechanical model. IEEE Transactions on Medical Imaging, 2001, 20, 1384-1397.	5.4	261
399	Serial Intraoperative Magnetic Resonance Imaging of Brain Shift. Neurosurgery, 2001, 48, 787-798.	0.6	367
400	<title>Real-time simulation and visualization of volumetric brain deformation for image-guided neurosurgery</title> ., 2001, , .		2
401	<title>Medical image segmentation using high-performance computer clusters</title> . , 2001, , .		1
402	<title>Multiresolution parameterization of meshes for improved surface-based registration</title> . , 2001, , .		3
403	Serial Intraoperative Magnetic Resonance Imaging of Brain Shift. Neurosurgery, 2001, 48, 787-798.	0.6	278
404	A Binary Entropy Measure to Assess Nonrigid Registration Algorithms. Lecture Notes in Computer Science, 2001, , 266-274.	1.0	21
405	Impaired Cerebral Cortical Gray Matter Growth After Treatment With Dexamethasone for Neonatal Chronic Lung Disease. Pediatrics, 2001, 107, 217-221.	1.0	351
406	Regional Magnetic Resonance Imaging Lesion Burden and Cognitive Function in Multiple Sclerosis. Archives of Neurology, 2001, 58, 115-21.	4.9	202
407	Surface Based Atlas Matching of the Brain Using Deformable Surfaces and Volumetric Finite Elements. Lecture Notes in Computer Science, 2001, , 1352-1353.	1.0	6
408	High Performance Computing in Image Guided Therapy. Informatik Aktuell, 2001, , 3-14.	0.4	0
409	Three-Dimensional Optical Flow Method for Measurement of Volumetric Brain Deformation from Intraoperative MR Images. Journal of Computer Assisted Tomography, 2000, 24, 531-538.	0.5	60
410	An image processing strategy for the quantification and visualization of exercise-induced muscle MRI signal enhancement. Journal of Magnetic Resonance Imaging, 2000, 11, 525-531.	1.9	26
411	Registration of 3D Intraoperative MR Images of the Brain Using a Finite Element Biomechanical Model. Lecture Notes in Computer Science, 2000, , 19-28.	1.0	49
412	Intraoperative Segmentation and Nonrigid Registration for Image Guided Therapy. Lecture Notes in Computer Science, 2000, , 176-185.	1.0	18
413	Pre- and Intra-operative Planning and Simulation of Percutaneous Tumor Ablation. Lecture Notes in Computer Science, 2000, , 317-326.	1.0	35
414	Deformable Modeling for Characterizing Biomedical Shape Changes. Lecture Notes in Computer Science, 2000, , 235-248.	1.0	19

#	Article	IF	CITATIONS
415	Virtual CT Cystoscopy. Investigative Radiology, 2000, 35, 331.	3.5	47
416	Periventricular white matter injury in the premature infant is followed by reduced cerebral cortical gray matter volume at term. Annals of Neurology, 1999, 46, 755-760.	2.8	506
417	Quantitative follow-up of patients with multiple sclerosis using MRI: Reproducibility. Journal of Magnetic Resonance Imaging, 1999, 9, 509-518.	1.9	83
418	3D Image Matching Using a Finite Element Based Elastic Deformation Model. Lecture Notes in Computer Science, 1999, , 202-209.	1.0	46
419	Quantitative follow-up of patients with multiple sclerosis using MRI: Reproducibility. , 1999, 9, 509.		15
420	A Volumetric Optical Flow Method for Measurement of Brain Deformation from Intraoperative Magnetic Resonance Images. Lecture Notes in Computer Science, 1999, , 928-935.	1.0	21
421	Fractional Segmentation of White Matter. Lecture Notes in Computer Science, 1999, , 62-71.	1.0	6
422	Nonlinear Registration and Template-Driven Segmentation. , 1999, , 67-84.		39
423	Quantitative magnetic resonance imaging of brain development in premature and mature newborns. Annals of Neurology, 1998, 43, 224-235.	2.8	596
424	A high performance computing approach to the registration of medical imaging data. Parallel Computing, 1998, 24, 1345-1368.	1.3	74
425	Multimodality deformable registration of pre- and intraoperative images for MRI-guided brain surgery. Lecture Notes in Computer Science, 1998, , 1067-1074.	1.0	28
426	Adaptive template moderated spatially varying statistical classification. Lecture Notes in Computer Science, 1998, , 431-438.	1.0	16
427	An Automated Registration Algorithm for Measuring MRI Subcortical Brain Structures. Neurolmage, 1997, 6, 13-25.	2.1	134
428	Fast k-NN classification for multichannel image data. Pattern Recognition Letters, 1996, 17, 713-721.	2.6	72
429	Laboratory Investigation:Automatic Identification of Gray Matter Structures from MRI to Improve the Segmentation of White Matter Lesions. Computer Aided Surgery, 1995, 1, 326-338.	1.8	7
430	Automatic identification of gray matter structures from MRI to improve the segmentation of white matter lesions. Journal of Image Guided Surgery, 1995, 1, 326-338.	0.4	146
431	Limited utility of structural MRI to identify the epileptogenic zone in young children with tuberous sclerosis. Journal of Neuroimaging, 0, , .	1.0	2